Molecular Biology and Evolution, 2025, **42**, 1–12
https://doi.org/10.1093/molbev/msaf303
Advance access publication 24 November 2025
Discoveries

MBE OXFORD

Accelerated Mitochondrial Genome Evolution in Parasitic Barnacles Driven by Adaptive and Non-adaptive Responses

Jibom Jung [1,†], **Siliang Song** [2,†], **Myeong-Yeon Kim** [3,†], **Haena Kwak** [4], **Benny K.K. Chan** [5], **Sun-Shin Cha** [3,6], **Ui Wook Hwang** [4,7,*], **Joong-Ki Park** [1,*]

[1]Division of EcoScience, Ewha Womans University, Seoul 03760, Korea
[2]Department of Ecology and Evolutionary Biology, University of Michigan, Ann Arbor, MI 48109, USA
[3]Department of Chemistry and Nanoscience, Ewha Womans University, Seoul 03760, Korea
[4]Department of Biology Education, Teachers College and Institute for Phylogenomics and Evolution, Kyungpook National University, Daegu 41566, Korea
[5]Biodiversity Research Center, Academia Sinica, Taipei 115, Taiwan
[6]Graduate Program in Innovative Biomaterials Convergence, Ewha Womans University, Seoul 03760, Korea
[7]Department of Advanced Bioconvergence, Kyungpook National University, Daegu 41566, Korea

[†]These authors contributed equally to this work.
***Corresponding authors:** E-mails: jkpark@ewha.ac.kr (JKP); uwhwang@knu.ac.kr (UWH)
Associate editor: Keith Crandall

Abstract

Parasitic lifestyles often impose profound evolutionary pressures, affecting molecular evolution through both adaptive and non-adaptive mechanisms. Among barnacles (subclass Cirripedia), the obligate parasitic Rhizocephala differ markedly from their filter-feeding thoracican relatives in morphology, ecology, and life history. However, how the shift to parasitism has shaped mitochondrial genome evolution within Cirripedia remains unclear. Here, we present the first comprehensive comparative analysis of mitochondrial genomes between parasitic and non-parasitic barnacles, including three newly sequenced and one unpublished species of parasitic Rhizocephala, a clade whose mitochondrial genomes had not been characterized until now. Phylogenomic and molecular evolutionary analyses reveal that Rhizocephala species exhibit extremely long branches likely attributed to the clade-specific tempo (high substitution rate) and mode (selection pressure) of mtDNA sequence evolution associated with their parasitic lifestyle. A two-cluster molecular clock test reveals significantly elevated substitution rates across rhizocephalans, consistent with reduced effective population sizes (N_e) linked to their opportunistic, host-dependent life cycles. We also detect signatures of positive selection in protein-coding genes encoding key components of the electron transport chain complexes III and IV. Structural modeling highlights amino acid substitutions at functionally critical sites for electron transfer and proton pumping, suggesting adaptive modifications to mitochondrial bioenergetics under hypoxic conditions within host tissues. Together, our findings underscore that both non-adaptive (genetic drift, relaxed selection) and adaptive (positive selection) processes have driven the rapid sequence divergence of mitochondrial genomes in parasitic Rhizocephala. Further experimental study is needed to elucidate how mitochondrial and nuclear-encoded subunits of oxidative phosphorylation coevolve in this specialized parasitic group.

Keywords: mitochondrial genome evolution, long branches, adaptive and non-adaptive responses, parasitic barnacles

Introduction

Molecular evolution, including patterns of nucleotide substitution, varies considerably across the living organisms due to the complex interplay of lineage-specific biological traits (e.g. life history traits) and environmental factors (e.g. habitat). Unraveling the molecular mechanisms underlying adaptive responses to varying lifestyles is a fundamental challenge in evolutionary biology. Comparisons of closely related taxa that occupy contrasting habitats or lifestyles offer insights into how natural selection shapes molecular evolution in response to specific ecological drivers (Bondareva et al. 2021; Martínez Sosa and Pilot 2023). Alongside adaptive changes, molecular evolution is shaped by a complex interplay of mutational forces, with non-adaptive processes (selectively neutral or nearly neutral) also contributing to the variation in the rates and patterns of genetic change across species with diverse biological traits. Comparing molecular evolutionary patterns between parasitic species and their closely related non-parasitic lineages offers a powerful framework for investigating how ecological specialization shapes the tempo and mode of sequence evolution. Parasitism is widespread across metazoans, having evolved independently over 200 times in at least 15 phyla (Weinstein and Kuris 2016; Luong and Mathot 2019). This lifestyle often involves dramatic shifts in life history traits, including high fecundity and degenerative changes in nonessential structures (Jennings and Calow 1975; Trouvé et al. 1998; Poulin 2011). Understanding the molecular evolution underpinning these evolutionary transformations within a robust phylogenetic framework is therefore critical to elucidating the genetic basis of evolutionary adaptation in parasitic life (Park et al. 2007).

Barnacles (the subclass Cirripedia) are sessile crustaceans with a unique cyprid larval stage characterized by a well-developed carapace covering the thorax vestige, distinguishing them

Received: June 30, 2025. **Revised:** November 9, 2025. **Accepted:** November 12, 2025
© The Author(s) 2025. Published by Oxford University Press on behalf of Society for Molecular Biology and Evolution.
This is an Open Access article distributed under the terms of the Creative Commons Attribution-NonCommercial License (https://creativecommons.org/licenses/by-nc/4.0/), which permits non-commercial re-use, distribution, and reproduction in any medium, provided the original work is properly cited. For commercial re-use, please contact reprints@oup.com for reprints and translation rights for reprints. All other permissions can be obtained through our RightsLink service via the Permissions link on the article page on our site—for further information please contact journals.permissions@oup.com.

Downloaded from https://academic.oup.com/mbe/article/42/12/msaf303/8340872 by ewhalib - (INACTIVE) user on 18 May 2026

from their sister clades (see Høeg et al. 2009). They are composed of three infraorders (Chan et al. 2021), showing clade-specific lifestyles: the burrowing Acrothoracica, the obligate parasitic Rhizocephala, and the non-parasitic, filter-feeding Thoracica (Glenner and Hebsgaard 2006). In particular, Rhizocephala exhibits a radical contrast to its closest thoracican relatives in their adult morphology, ecology, and life-history traits. Rhizocephalans exhibit extensive morphological modifications associated with their parasitic lifestyle, including the degeneration of multiple internal organ systems (e.g. respiratory, digestive, sensory, and excretory). Instead, they possess two highly specialized body structures: (1) the interna, a root-like network that infiltrates the tissues of crustacean hosts, and (2) the externa, a membranous sac that typically protrudes from the host's abdomen and serves primarily for reproduction (Høeg 1992; Øksnebjerg 2000; Høeg et al. 2009 ; Miroliubov et al. 2019, 2022). Adult rhizocephalans lack external feeding and independent respiratory structures, instead relying on their internal rootlet system (the interna) to absorb nutrients and decapod hosts' respiratory systems (O'Brien and Van Wyk 1985; Bresciani and Høeg 2001 ; Miroliubov et al. 2020). Molecular phylogenetic analyses based on various genetic markers—including 18S and 28S rDNAs, histone H3, mtDNA Cox1, and 16S rDNA—have consistently placed Rhizocephala as a derived clade within Cirripedia, with Thoracica identified as their closest sister group (Schram 1986; Spears et al. 1994; Pérez-Losada et al. 2009; Lin et al. 2016). Despite advances in our understanding of their ecological traits and phylogenetic relationships, relatively very little is known about how their parasitic lifestyle has shaped the evolution of mitochondrial genomes (mtDNA).

Mitochondrial protein-coding genes (PCGs) encode core components of the oxidative phosphorylation system, which drives ATP production via the electron transport chain (ETC). These genes are also widely used for phylogenetic inference due to their conserved gene content (Wolstenholme 1992; Boore 1999). However, until now, mtDNA data for Cirripedia have been heavily biased toward Thoracica (68 species as of April 2025), with no representative from the parasitic Rhizocephala clade published to date. This sampling bias obscures the potential impacts of parasitism on mitochondrial genome evolution in barnacles. To address this gap, we sequenced the complete mtDNA of three rhizocephalans (*Sacculina confragosa, Parasacculina yatsui*, and *Parasacculina shiinoi*), incorporated an additional unpublished sequence of *Sacculina lata*, and conducted comparative analyses across Cirripedia, focusing on the interplay among mutation rates, nucleotide compositional bias, and selection pressures associated with their highly specialized parasitic lifestyle. To this end, using mtDNA sequence data, we (1) reconstructed phylogenetic relationships within Cirripedia, (2) examined patterns of molecular evolution (including elevated substitution rates, relaxed purifying selection, or gene order changes), and (3) investigated signatures of positive selection in ETC genes, potentially reflecting molecular adaptations to the hypoxic environment imposed by an obligate parasitic lifestyle.

Results

General Features of Rhizocephala mtDNA

The newly sequenced rhizocephalan mitogenomes range in size from 15,982 bp (*S. confragosa*) to 18,050 bp (*P. shiinoi*), encoding 37 mitochondrial genes (13 PCGs, 22 tRNAs, and 2 rRNAs) similar to those found in Thoracica species, except that *P. shiinoi* lacks one tRNA gene (*trnS2*) (Figs S1 and S2). The nucleotide composition and AT/GC skews of the 13 PCGs in four Rhizocephala species (three newly sequenced and one unpublished *S. lata* sequence from GenBank, accession no. MZ411548) differ substantially from those of Thoracica (Table S1). Rhizocephala species show a strong bias toward higher T and lower C content (average nucleotide composition: 50.22% T, 26.13% A, 15.06% G, and 8.59% C), with an average AT skew of −0.32 and GC skew of 0.27. In contrast, Thoracica species exhibit a weaker AT skew (−0.18) and a negative GC skew (−0.03) (Table S1; Fig. S3a and b). Interestingly, nucleotide compositional bias varies considerably even within Rhizocephala, with AT skew ranging from −0.40 to −0.19 and GC skew from 0.12 to 0.41. The extremely long branches observed among Rhizocephala species in phylogenetic trees likely result from this within-group variation in nucleotide composition bias (see Results and Discussion for more details). Consistent with the stark differences in nucleotide composition, the amino acid composition of the 13 PCGs in Rhizocephala also differs markedly from that of Thoracica (Fig. S4a and b). Furthermore, mitochondrial gene orders of Rhizocephala species are highly variable and deviate significantly from the conserved pancrustacean ground plan, which is also retained in thoracican barnacles (Fig. S5) (Podsiadlowski and Bartolomaeus 2005; Yang and Yang 2008; Ki et al. 2009). Phylogenetic analysis based on gene order information placed Rhizocephala in a distinct cluster with notably longer branches than Thoracica species (Fig. S6), suggesting accelerated mtDNA evolution and extensive rearrangements since diverging from their common ancestor with Thoracica.

Phylogenetic Relationships Within Cirripedia and Exceptionally Long Branches in Rhizocephala

Both maximum likelihood (ML) and Bayesian inference analyses —particularly under the site-heterogeneous CAT model and excluding third codon positions—recovered two well-supported monophyletic clades (100% ML bootstrap, and 1.0 Bayesian posterior probability values, in ML and Bayesian inference analyses, respectively), each representing Rhizocephala and Thoracica (Fig. 1). Within Thoracica, family-level groupings were largely monophyletic (e.g. Tetraclitidae, Chthamalidae), although Balanidae was not entirely resolved, as *Armatobalanus allium* clustered with pyrgomatids (*Pyrgopsella annandalei, Savignium* sp., and *Nobia grandis*). Within Rhizocephala, sacculinid species (*Sacculina* spp.) and polyascid species (*Parasacculina* spp.) each formed strongly supported subclades. Phylogenetic relationships within each group are not described in detail, as they lie beyond the primary scope of this study. Nevertheless, it is noteworthy that all Rhizocephala species exhibit exceptionally long branches, indicative of elevated substitution rates.

Accelerated Mitochondrial Sequence Evolution in Parasitic Rhizocephala

The two-cluster molecular clock test revealed that the molecular substitution rate is significantly higher in the rhizocephalan clade than the thoracican clade ($Z = 20.8$, $P = 4.3 \times 10^{-96}$). Specifically, from the shared node where the Rhizocephala diverged from Thoracica, the mean branch length to the terminal tips was much longer in the rhizocephalan clade ($d = 0.406$ substitutions per site) than that in the thoracican clade ($d = 0.098$ substitutions per site), resulting in a difference of $\Delta d = 0.308$ (SE = 0.015) substitutions per site between the two groups. These results indicate that the rhizocephalans

Downloaded from https://academic.oup.com/mbe/article/42/12/msaf303/8340872 by ewhalib - (INACTIVE) user on 18 May 2026

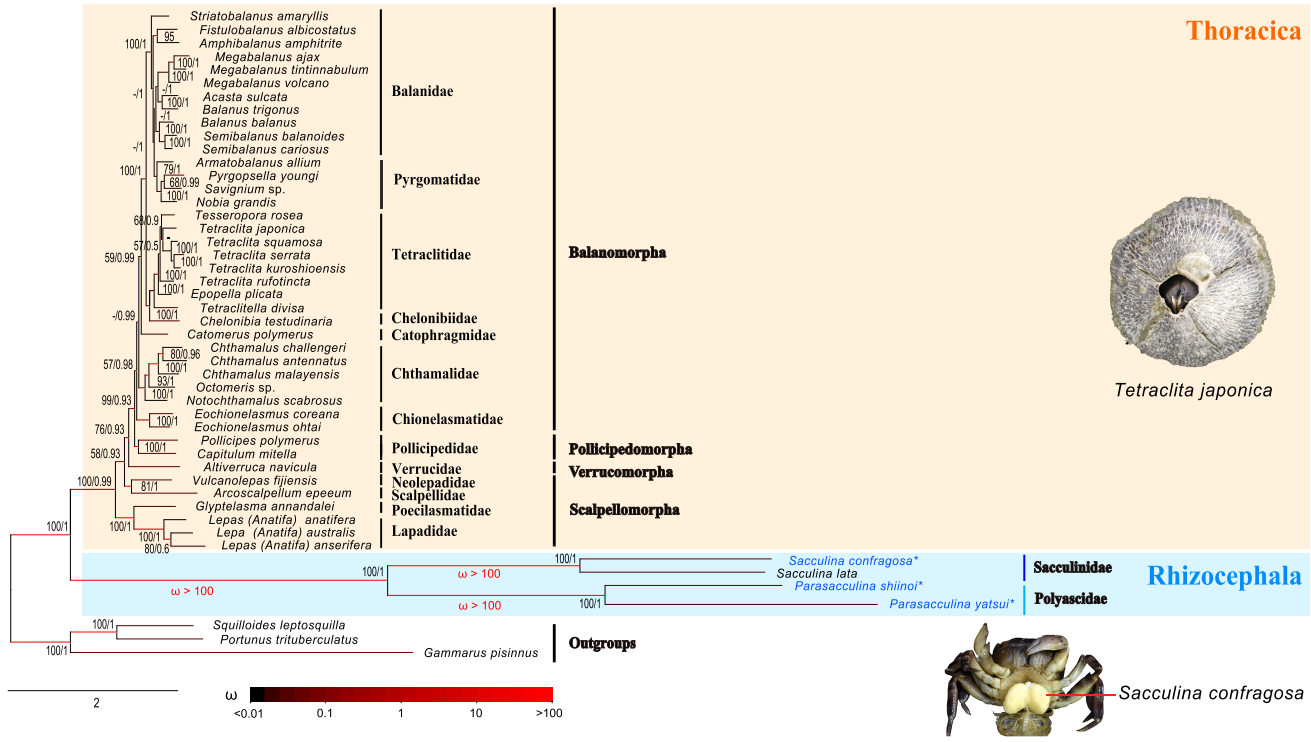


Fig. 1. Mitochondrial genome phylogeny of the Cirripedia (including 4 Rhizocephala and 41 Thoracica species) based on the first and second codon sequences of 13 PCGs (excluding 3rd codon position sequences) using maximum likelihood with the CAT model and Bayesian methods. Maximum likelihood bootstrap/Bayesian posterior probability values are represented near the branches. *: newly determined mitochondrial genome sequences in this study. Estimated d_N/d_S ratios (ω) are shown for each branch in the Cirripedia phylogenetic tree. All 13 PCGs are used to estimate d_N/d_S and length of each branch. Branch lengths represent the expected number of nucleotide substitutions per site along each branch (scale bar = 2 substitutions/site). $d_N/d_S > 1$ in the rhizocephalan clade are shown near the corresponding branches.

have evolved at approximately 4.14 times higher substitution rate than that observed in Thoracica species. The results from the two-cluster molecular clock test demonstrate pronounced rate heterogeneity in cirripede mtDNA, with parasitic Rhizocephala exhibiting markedly accelerated evolution compared to their filter-feeding relatives.

To assess whether this acceleration is specific to mitochondrial genes or reflects a broader genomic pattern potentially driven by reduced effective population size (N_e), we extended our analysis to a nuclear gene marker. We reconstructed an ML phylogeny using the V5–V7 region of 18S rDNA sequences from 65 species of Rhizocephala and Thoracica (see Materials and methods section for details) and applied the same two-cluster molecular clock test. Consistent with the results from mitochondrial genes, we found that substitution rates in Rhizocephala were also significantly elevated at the 18S locus compared to Thoracica ($Z = 8.80$, $P = 0.0004$). Although 18S rDNA is one of the most slowly evolving nuclear genes, the observed rate acceleration in this marker provides strong evidence that the substitution rate acceleration is not confined to the mitochondrial genome. Taken together, these results suggest that the elevated substitution rates detected in both mitochondrial and nuclear genes are likely driven, at least in part, by genome-wide processes such as relaxed purifying selection under reduced effective population size (N_e), a characteristic often associated with obligate parasitism rather than by mitochondrial-specific evolutionary drivers alone.

Selection Pressure Shifts in Rhizocephala

To overview the shift of selection pressure within the Cirripedia phylogeny, we used CodeML in PAML (Yang 2007) to estimate the ratio of non-synonymous to synonymous substitution rate (d_N/d_S) at each branch. Our statistical test of selection signals turns out that the internal branches of the rhizocephalan clade show very high d_N/d_S (Fig. 1), indicating a rapid adaptive sequence evolution during their early stage of speciation in the rhizocephalan clade. We also implemented BUSTED (Murrell et al. 2015) and RELAX (Wertheim et al. 2015) in HyPhy (Kosakovsky Pond et al. 2020) to further separate the effect of the site-level positive selection and the branch-level relaxation/intensification of selection pressure within the rhizocephalan clade. When the 13 PCGs were concatenated, we detected both site-level positive selection ($P = 4.27 \times 10^{-19}$) as well as branch-level relaxation of selection ($P = 2.00 \times 10^{-92}$) (Tables 1 and 2) in the rhizocephalan clade. On the other hand, when each of the 13 PCGs was analyzed separately, we found positive selection signals in Cyt *b*, Cox1, and Cox3 (Table 2), and the signals of relaxation of purifying selection in Atp8, Cox1, Cox2, and Cox3, respectively (Table 1). In contrast, the positive selection signal is not strong in the thoracican clade, neither for the concatenated 13 PCGs nor for any of the 13 individual PCGs (only Nad4 has $P = 0.01$, but is not significant with multiple testing adjustment) (Table 2).

Positive Selection in Key Mitochondrial ETC Genes in Rhizocephala

Despite pervasive relaxation of purifying selection, we also detected site-level positive selection in three PCGs (Cyt *b*, Cox1, and Cox3), key components of the mitochondrial ETC, exclusively in Rhizocephala species, but not in Thoracica species (Table 2). Structural modeling identified 17 amino acid substitutions: 9 in the cytochrome *b* (Cyt *b*) subunit of the

Downloaded from https://academic.oup.com/mbe/article/42/12/msaf303/8340872 by ewhalib - (INACTIVE) user on 18 May 2026

Table 1. Relaxed purifying selections within rhizocephalan clade among 13 PCGs detected by RELAX

Gene	LRT	*K*	*P*	ω_rh	ω_th
All 13 PCGs	415.76	0.93	2.00E-92[a]	0.0734	0.0463
Atp6	0	1	1	0.2763	0.0237
Atp8	13.91	0	0.000192[a]	0.9912	0.0856
Cyt *b*	0.38	0.945661	0.536635	0.2209	0.0184
Cox1	18.74	0.927581	1.50E-05[a]	0.0453	0.0094
Cox2	6.95	0.333154	0.008379[a]	0.0231	0.0133
Cox3	32	3.96E-08	1.54E-08[a]	0.3931	0.0309
Nad1	0.38	1.021568	0.535171	0.0271	0.0336
Nad2	−0.0016	1	1	0.4357	0.0334
Nad3	0.75	0.995721	0.385884	0.0503	0.0193
Nad4	3.18	0.578697	0.074644	0.0796	0.0529
Nad4L	2.27	0.58808	0.131654	0.1746	0.0481
Nad5	−0.0002	1	1	0.0593	0.0488
Nad6	0.0027	0.993915	0.958384	0.5451	0.0348

K, relaxation parameter. $K < 1$ means selection relaxation, $K > 1$ means selection intensification, $K = 1$ means selection pressure unchanged, ω_rh, the global d_N/d_S ratio among the Rhizocephala species; ω_th, the global d_N/d_S ratio among the Thoracica species.
[a]Statistically significant.

cytochrome *bc1* complex (ETC complex III, Cyt *bc1*), and 8 in the subunits of cytochrome *c* oxidase (ETC complex IV, COX), specifically 7 in Cox1 and 1 in Cox3 (Fig. 2a). Both Cyt *bc1* and COX, membrane-bound components of the ETC, play a crucial role in facilitating proton pumping from the mitochondrial matrix (N-side) to the intermembrane space (P-side), driving the electrochemical gradient required for ATP synthesis (Fig. 2b). Electron transfer in Cyt *b* occurs via two sequential pathways: a primary pathway from the Qo site to the Qi site via hemes bL and bH, and a secondary pathway from the Qo site to Cyt *c1* via the [2Fe2S] iron–sulfur protein (ISP) (Fig. 2b). Note that six of the amino acid changes in Cyt *b* (N41, F54, Y56, M86, L125, and F126) are located within the heme bL binding site, which is engaged in the primary electron transfer pathway (Fig. 3a). In addition, a substitution at position 171 resides at the interface with the [2Fe2S] ISP, which mediates the secondary electron transfer pathway (Fig. 3a). In Rhizocephala species, seven amino acid substitutions were identified in Cox1 (S21, I34, R41, G49, L72, S170, and F273), and one in Cox3 (S195) (Fig. 3b). Four amino acid changes (S21, 34I, R41, and L72) were also found in helices I and II of Cox1, which are involved in heme binding. Furthermore, a highly conserved aspartate near the H-channel (D51 in bovine, D49 in Thoracica) is replaced by glycine (G49) in Rhizocephala, occupying a structurally equivalent position in helix II adjacent to the H-channel, a region critical for proton pumping (Fig. 3c).

Discussion

Mitochondrial Evidence for Rapid Evolution in Rhizocephala

The mitochondrial genome phylogeny of the Cirripedia reveals two well-supported monophyletic clades, Rhizocephala and Thoracica (Fig. 1), that are consistent with previous phylogenetic studies based on morphology and 18S rDNA (Glenner and Hebsgaard 2006; Høeg et al. 2020), as well as with a recent synthetic classification framework for the Cirripedia (Chan et al. 2021). Most notably, unlike Thoracica species, all Rhizocephala species exhibit exceptionally long branches in the mitochondrial phylogenetic tree including internal nodes connecting individual species, indicating markedly elevated nucleotide substitution rates

Table 2. Positive selections within rhizocephalan clade among 13 PCGs detected by BUSTED

Gene	ω_1_rh (fraction)	ω_2_rh (fraction)	ω_3_rh (fraction)	LRT_rh	*P*_rh (ω_3_rh > 1)	ω_1_th (fraction)	ω_2_th (fraction)	ω_3_th (fraction)	LRT_th	*P*_th (ω_3_th > 1)
All 13 PCGs	0.002 (0.48)	0.13 (0.38)	75.42 (0.14)	79.74	4.27E-19	0.00 (0.58)	0.01 (0.41)	1.00 (0.00)	NA	NA
Atp6	0.00 (0.58)	0.63 (0.42)	1.00 (0.00)	NA	NA	0.00 (0.75)	0.01 (0.24)	1.00 (0.12)	NA	NA
Atp8	0.18 (0.27)	0.18 (0.58)	3.25 (0.15)	0.76	0.342631	0.00 (0.41)	0.05 (0.59)	1.00 (0.00)	NA	NA
Cyt *b*	0.01 (0.80)	0.99 (0.15)	31999.90 (0.05)	26.81	7.54E-07	0.00 (0.66)	0.004 (0.34)	1.00 (0.00)	NA	NA
Cox1	0.00 (0.73)	0.31 (0.21)	64.05 (0.06)	35.4	1.03E-08	0.00 (0.00)	0.002 (1.00)	1.00 (0.00)	NA	NA
Cox2	0.00 (0.74)	0.03 (0.17)	133.48 (0.09)	6.27	0.022	0.00 (0.93)	0.01 (0.07)	1.00 (0.00)	NA	NA
Cox3	0.01 (0.68)	0.97 (0.17)	455.67 (0.14)	47.88	2.01E-11	0.00 (0.96)	0.09 (0.04)	1.00 (0.00)	NA	NA
Nad1	0.00 (0.37)	0.02 (0.50)	1.00 (0.13)	NA	NA	0.01 (0.98)	0.09 (0.02)	1.00 (0.00)	NA	NA
Nad2	0.01 (0.59)	0.57 (0.27)	9999999171 (0.13)	−0.11	1	0.00 (0.39)	0.01 (0.61)	1.00 (0.01)	NA	NA
Nad3	0.00 (0.33)	0.06 (0.42)	2.79 (0.26)	−1.78	1	0.00 (0.51)	0.01 (0.49)	1.00 (0.00)	NA	NA
Nad4	0.00 (0.48)	0.03 (0.39)	1.00 (0.13)	NA	NA	0.00 (0.61)	0.02 (0.39)	9.49 (0.004)	7.77	0.01
Nad4L	0.00 (0.54)	0.05 (0.46)	1.00 (0.00)	NA	NA	0.00 (0.63)	0.03 (0.37)	1.28 (0.00)	NA	NA
Nad5	0.00 (0.45)	0.02 (0.41)	401.00 (0.15)	−0.46	1	0.00 (0.45)	0.01 (0.55)	1.04 (0.01)	−0.54	1
Nad6	0.01 (0.49)	0.17 (0.26)	12.80 (0.25)	9.12	0.0052	0.00 (0.28)	0.01 (0.71)	1.00 (0.01)	NA	NA

ω_1_rh, ω_2_rh, and ω_3_rh are the three d_N/d_S ratios estimated in the Rhizocephala clade (when the Rhizocephala clade is set as the foreground clade), with restriction ω_1_rh ≤ ω_2_rh ≤ 1 ≤ ω_3_rh.
ω_1_th, ω_2_th, and ω_3_th are the three d_N/d_S ratios estimated in the Thoracica clade (when the Thoracica clade is set as the foreground clade), with restriction ω_1_th ≤ ω_2_th ≤ ω_3_th.
The likelihood ratio test (LRT_rh or LRT_th) is conducted against the null model where ω_3_rh = 1 (when the Rhizocephala clade is set as the foreground clade) or ω_3_th = 1 (when the Thoracica clade is set as the foreground clade).
Some LRT and *P* values are shown as NA because ω_3_rh ≤ 1 (or ω_3_th ≤ 1), which implies no positive selection in the Rhizocephala (or Thoracica) clade, so the test is not needed.

Downloaded from https://academic.oup.com/mbe/article/42/12/msaf303/8340872 by ewhalib - (INACTIVE) user on 18 May 2026

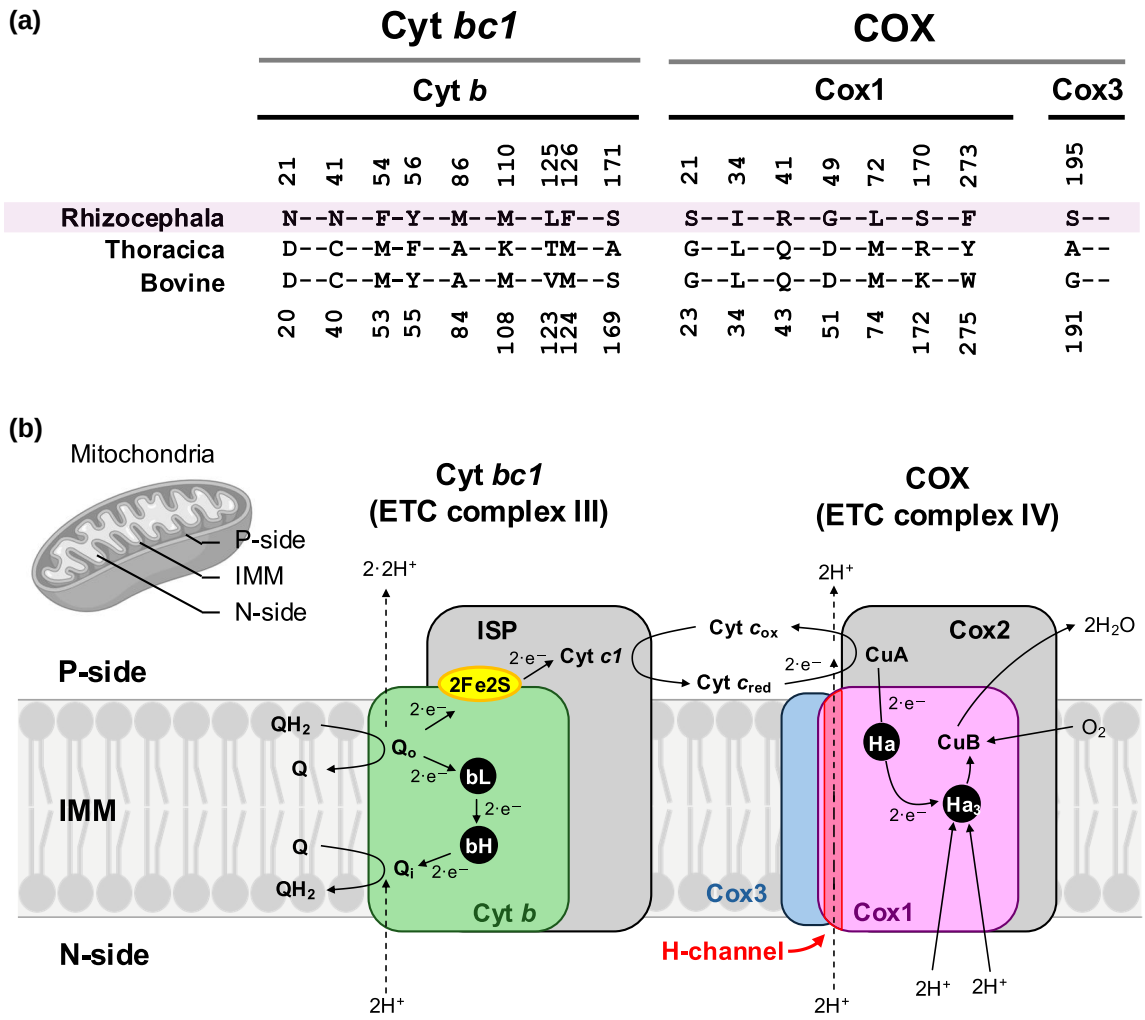


Fig. 2. Amino acid substitutions and structural context of mitochondrial electron transport chain (ETC) complexes III and IV in Rhizocephala. a) Alignment of partial amino acid sequences of cytochrome *b* (Cyt *b*), cytochrome *c* oxidase subunit I (Cox1), and subunit III (Cox3) across Rhizocephala, Thoracica, and Bovinae. Positively selected and functionally relevant amino acid substitutions in Rhizocephala are highlighted at key positions associated with electron transfer and proton pumping. Notable substitutions occur in conserved regions, including heme bL binding site of Cyt *b* and helices involved in heme coordination of Cox1. b) Schematic representation of mitochondrial ETC complex III (cytochrome *bc1*, Cyt *bc1*) and complex IV (cytochrome *c* oxidase, COX) embedded in the inner mitochondrial membrane (IMM) that displays electron transport pathways (black arrows) and associated proton translocation across the membrane (black dashed arrows). The core subunits—Cyt *b* in ETC complex III and Cox1 and Cox3 in ETC complex IV—are shown in green, blue, and pink, respectively. The ISP and cytochrome *c* oxidase subunit II (Cox2) are shaded in grey. Key structural elements involved in electron transfer include the [2Fe-2S] cluster of the ISP, the heme centers (bL and bH) of Cyt *b*, and the CuA, CuB, and heme centers (Ha, Ha_3) of Cox1. The red arrow indicates the H-channel, where the Asp51-to-Gly49 substitution in Rhizocephala species is discovered.

(see the following section for more information). Furthermore, the mtDNA of Rhizocephala species show strikingly high variability in gene order, characterized by extensive rearrangements that stand in stark contrast to the highly conserved pancrustacean ground pattern observed in Thoracica species (Podsiadlowski and Bartolomaeus 2005; Yang and Yang 2008; Ki et al. 2009; Fig. S5). These pronounced gene order changes, together with the presence of phylogenetically deep and unusually long branches—even among closely related congeneric taxa such as *Sacculina* and *Parasacculina*—provide compelling evidence for an accelerated rate of mitochondrial genome evolution within the Rhizocephala clade following their divergence from the most recent common ancestor shared with Thoracica.

Accelerated Mitochondrial Sequence Evolution Driven by Non-adaptive Processes in Parasitic Rhizocephala

The most notable features of our mitochondrial phylogeny are the presence of exceptionally long branches across all rhizocephalan species, compared to those in Thoracica (Fig. 1). The mean branch length for Rhizocephala ($d = 0.406$ substitutions per site) is approximately 4.14-fold longer than that of Thoracica ($d = 0.098$ substitutions per site), indicating accelerated molecular evolution in the parasitic Rhizocephala clade. This notable disparity suggests clade-specific evolutionary mechanisms, including an elevated substitution rate and shifts in selective pressures, potentially driven by adaptations to their parasitic lifestyle. Such mitochondrial divergence aligns with broader patterns of variation in nucleotide substitution rates and selection signals across taxa, which are shaped by ecological (e.g. life history strategies), physiological (e.g. metabolic demands), and evolutionary (e.g. relaxed purifying selection) factors. Substitution rate variation is frequently associated with life history traits such as body size, generation time, and reproductive mode (Gillooly et al. 2005; Bromham 2009). Parasitic lineages, including lice (Page et al. 1998), fish lice (Hassanin 2006), chalcidoid wasps (Xiao et al. 2011), parasitic plants (Bromham et al. 2013), and bopyrid isopods (An et al. 2020),

Downloaded from https://academic.oup.com/mbe/article/42/12/msaf303/8340872 by ewhalib - (INACTIVE) user on 18 May 2026

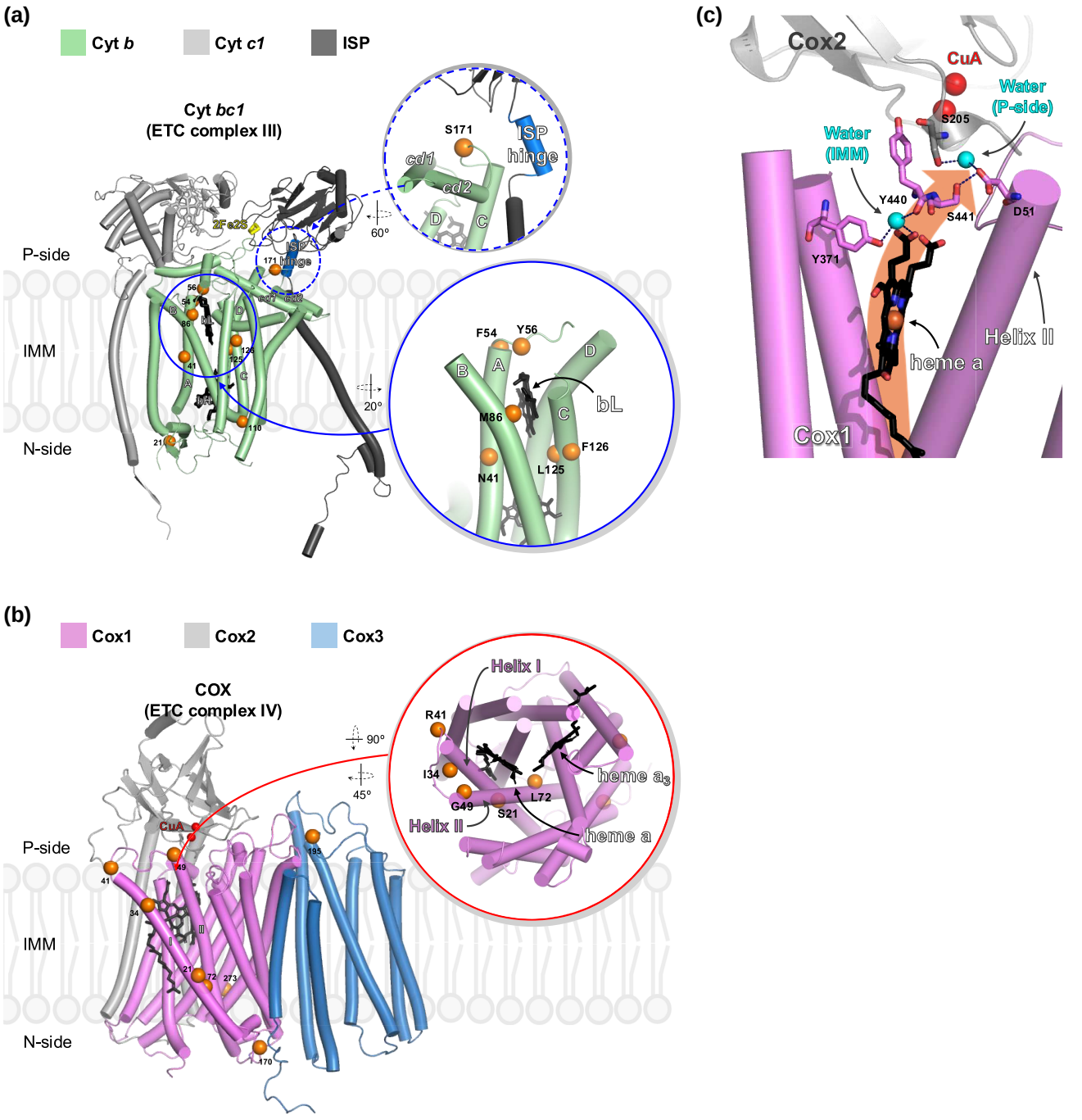


Fig. 3. Distribution of positively selected sites in the ETC complexes III and IV in Rhizocephala species and hydrogen-bonding network of H-channel in Cox1. a) Cyt *b*, Cyt *c1*, and ISP in one monomer are represented as cylindrical helices in green, light grey, and dark grey, respectively. The Cα atoms of 9 positively selected sites are marked as orange spheres, with numbers indicating amino acid residue positions. The prosthetic heme groups (bL and bH) in Cyt *b* are shown in black, and the 2Fe2S cluster of ISP is depicted as yellow sticks. The blue-dashed circle highlights the location of S171 near the ISP hinge region, and the blue-lined circle is a zoomed-in view of the bL site, showing four helices (A to D) with 6 mutation points (N41, F54, Y56, M86, L125, and F126). In Thoracica, these residues correspond to C41, M54, F56, A86, T125, M126, and A171, respectively. b) Cox1, Cox2, and Cox3 in one monomer are represented in pink, light grey, and blue, respectively. The Cα atoms of 8 positively selected points in Cox1 and Cox3 are shown as orange spheres with the residue numbers. Two copper ions in the bi-nuclear CuA center of Cox2 are depicted as red spheres, and the prosthetic heme groups (heme a and heme a3) in Cox1 are represented as black sticks. The red-lined circle shows a top view of Cox1 from the P-side, highlighting 5 positively selected amino acid residues (S21, I34, R41, G49, and L72) in helix I and helix II around heme a. In Thoracica, these residues correspond to G21, L34, Q41, D49, and M72. c) Zoomed-in view of the H-channel in cytochrome *c* oxidase subunit I (Cox1) of the bovine, highlighting key residues involved in proton transfer and the hydrogen-bonding network. Residues participating in the hydrogen-bonding network, along with the porphyrins of heme a, are represented as stick models and labeled accordingly. In the stick representations, oxygen and nitrogen atoms are colored red and blue, respectively. Iron and copper ions are shown as brown and red spheres, respectively. Water molecules are depicted as cyan spheres and are labeled according to their locations: Water (P-side) and Water (IMM). Hydrogen bonds are indicated by dashed lines. The orange arrow illustrates the overall direction of proton transfer along the H-channel. The protein structure, heme cofactor, and water molecules were visualized using the coordinates of fully reduced bovine cytochrome *c* oxidase (PDB ID: 2EIK).

Downloaded from https://academic.oup.com/mbe/article/42/12/msaf303/8340872 by ewhalib - (INACTIVE) user on 18 May 2026

have consistently shown elevated evolutionary rates relative to free-living relatives. Rhizocephala species exhibit some life history characteristics that likely contribute to their elevated mitochondrial substitution rates. Notably, compared to thoracican barnacles, rhizocephalans undergo fewer larval stages (4 to 5 vs. 6 naupliar instars) and complete development more rapidly (4 to 5 days vs. 14 to 21 days) (Chan 2003 ; Chan et al. 2005).

The elevated nucleotide substitution rate in rhizocephalan species is also likely driven by their smaller effective population sizes (N_e), a consequence of their parasitic lifestyle, in contrast to the non-parasitic, filter-feeding Thoracican species. According to the nearly neutral theory (Ohta 1973), reduced N_e weakens the efficacy of purifying selection, allowing mildly deleterious mutations to persist and thereby accelerating the overall substitution rate. Consistent with this theoretical expectation, our analyses detected a significant relaxation of purifying selection across all 13 mitochondrial PCGs in Rhizocephala ($P = 2 \times 10^{-92}$; Table 1). The selection intensity parameter ($K = 0.93$) indicates that the d_N/d_S (ω) ratio in Rhizocephala is shifted toward neutrality compared to Thoracica. Specifically, the global d_N/d_S ratio was higher in Rhizocephala ($\omega = 0.073$) than in Thoracica ($\omega = 0.046$) for the entire 13 PCG sequences, and relaxation of purifying selection was particularly pronounced in four genes (Atp8, Cox1, Cox2, and Cox3; Table 1). These patterns are consistent with findings from other parasitic metazoans, which frequently exhibit reduced N_e due to their opportunistic, host-dependent life cycles—where successful reproduction is often limited by stochastic events and host availability (Shokri Bousjein et al. 2016; Strobel et al. 2019). Indeed, compared to Thoracica, Rhizocephala species are sparsely distributed and often clustered within highly localized host populations and exhibit abbreviated larval development (Chan et al. 2005), further constraining population size and genetic connectivity. Such ecological constraints (reduced N_e and limited spatial distribution) intensify genetic drift and are likely to promote relaxed purifying selection (Dowton and Austin 1995; Ebert 1998; Page et al. 1998; Bromham et al. 2013). This provides a compelling explanation for the exceptionally long branches observed in rhizocephalan mitochondrial phylogenies, which are interpreted as a non-adaptive consequence of their parasitic lifestyle (Fig. 1).

Adaptive Evolution of Mitochondrial ETC Genes in Parasitic Rhizocephala

The obligate parasitic lifestyle of Rhizocephala is a unique evolutionary innovation within Cirripedia and likely played a key role in their diversification, accompanied by altered selection pressures associated with their parasitic life. This transition to parasitism is expected to impose distinct metabolic and physiological constraints, particularly those related to oxygen acquisition and energy metabolism, thereby altering selection pressures on mitochondrial function. Supporting this view, our statistical test of selection pressure across all 13 PCGs revealed notably elevated d_N/d_S ratios along internal branches of the Rhizocephala clade (Fig. 1), suggesting that adaptive sequence evolution accompanied their initial transition to parasitic lifestyle during the early diversification of the rhizocephalan clade. In particular, we detected signatures of positive selection in several key mitochondrial genes, including Cyt *b*, Cox1, and Cox3 (Table 2) in Rhizocephala species, which encode essential components of the mitochondrial ETC complexes—complex III (cytochrome *bc1* complex, Cyt *bc1*) and complex IV (cytochrome *c* oxidase, COX) (Fig. 2). These complexes are central to oxidative phosphorylation, facilitating electron transfer and proton translocation for ATP production (Sazanov 2015; Sharma et al. 2017). The observed positive selection signals likely reflect adaptive modifications that may optimize ETC function in response to oxygen-limited conditions imposed by their parasitic lifestyle.

Previous studies have shown that positive selection in mitochondrial genes often corresponds to adaptive responses to challenging environments, such as high altitudes (Xu et al. 2005; da Fonseca et al. 2008), hypoxic habitats (Luo et al. 2008), and hydrothermal vents (Yang et al. 2019; Zhang et al. 2020; Zhang et al. 2021). In these contexts, nonsynonymous amino acid substitutions can modulate ETC efficiency, enabling metabolic flexibility under low-oxygen conditions (Chandel et al. 1997; Guzy and Schumacker 2006; Timón-Gómez et al. 2020). Rhizocephalans, lacking independent respiratory organs, rely entirely on host-mediated oxygen supply through their internal root-like structures (O'Brien and Van Wyk 1985; Bresciani and Høeg 2001). A recent report documented that two Rhizocephala species simultaneously infested a single host crab, likely exacerbating oxygen-lacking environment within the host, due to increased metabolic burden from multiple parasite loads (Golubinskaya et al. 2021). This dependence likely results in persistent hypoxic stress, driving adaptive changes to mitochondrial function. In support of this, we identified amino acid substitutions in ETC complex III (Cyt *b* gene in cytochrome *bc1*) and complex IV (Cox 1 and Cox3 genes in cytochrome *c* oxidase) in Rhizocephala that are functionally associated with electron transport efficiency. The cytochrome *bc1* complex comprises three key catalytic components: cytochrome *b* (Cyt *b*, which contains the bL and bH heme groups), the [2Fe–2S] ISP, and cytochrome *c1* (Cyt *c1*). These components coordinate electron transfer through the Q-cycle, shuttling electrons from ubiquinol (QH_2, the reduced form of coenzyme Q) to Cyt *c1*. The electrons are transferred to Cyt *c1* and ultimately to cytochrome *c* oxidase, the terminal enzyme responsible for proton (H^+) translocation from the mitochondrial matrix (N-side) to the intermembrane space (P-side) (Fig. 2b). This proton gradient drives ATP synthesis via oxidative phosphorylation. Note that six amino acid changes in Cyt *b* (N41, F54, Y56, M86, L125, and F126) of complex III occur within bL heme-binding site involved in primary electron transfer via the Q-cycle (Figs 2 and 3a). These substitutions may influence redox activity or alter electron transfer kinetics. Additionally, a notable hydrophobic-to-hydrophilic amino acid substitution at position 171 [Alanine (A)→Serine (S)] in Cyt *b* occurs at the interface with the [2Fe2S] ISP, a component known to influence inter-subunit electron flow. The ISP is located at the interface between the membrane and the P-side of the mitochondrion, and thus an amino acid change may influence electron delivery efficiency between catalytic subunits, potentially affecting the secondary electron transfer pathway. Experimental evidence demonstrated that amino acid changes near the ISP hinge region can significantly impact their catalytic activity (Darrouzet et al. 2000).

Similarly, in complex IV (cytochrome *c* oxidase, COX), we identified seven amino acid substitutions in Cox1 (S21, I34, R41, G49, L72, S170, and F273) and one in Cox3 (195S) (Figs 2a and 3b). Four substitutions (e.g. S21, 34I, R41, and L72) are located within helices I and II of Cox1, the regions that coordinate heme binding and electron transfer to oxygen molecules (Fig. 3b). Of particular interest is the replacement of

Downloaded from https://academic.oup.com/mbe/article/42/12/msaf303/8340872 by ewhalib - (INACTIVE) user on 18 May 2026

a conserved aspartate residue (51D; negatively charged) with glycine (G49; non-polar) within the H-channel of Cox1 (Fig. 2a). In bovines, this aspartate stabilizes a hydrogen-bonding network involving water molecules and conserved residues (S205, Y371, Y440, and S441; Fig. 3c) that is essential for coupling redox reactions to proton pumping, a fundamental process in ATP synthesis (Sharma et al. 2017; Zdorevskyi et al. 2023). Substituting D51 with G49 in Rhizocephala could affect hydrogen-bonding network, potentially modulating the efficiency of the redox-driven proton translocation.

The amino acid changes identified in ETC complexes III and IV likely represent adaptive or compensatory modifications that enable Rhizocephala species to modulate mitochondrial function under the chronic oxygen limitation imposed by their parasitic life. As rhizocephalans lack independent respiratory structures and rely entirely on their hosts' respiratory systems, they are exposed to low-oxygen conditions within host tissues (O'Brien and Van Wyk 1985; Bresciani and Høeg 2001). Under such constraints, the amino acid substitutions observed may favor modifications that optimize ETC performance under oxygen-limited conditions. These adaptations may modulate energy production efficiency, mitigate reactive oxygen species formation, and maintain ATP output, reflecting functional optimization in response to the metabolic demands of host-dependent parasitic life. However, it remains unclear whether these substitutions enhance ETC performance or instead reflect a downregulation of mitochondrial bioenergetics in response to the reduced metabolic demands associated with their parasitic lifestyle. Although we detected statistically significant signals of positive selection in several mitochondrial ETC genes, these results should be interpreted with caution, as d_N/d_S-based signatures alone are not sufficient to definitely confirm adaptive evolution. As noted in a recent review (Müller et al. 2012), many eukaryotes inhabiting oxygen-poor environments undergo metabolic reshaping of mitochondrial function, such as metabolic repression by reducing reliance on ETC-mediated ATP production, without necessarily involving amino acid changes that enhance protein function (Hand and Hardewig 1996; Hochachka et al. 1996). Thus, the amino acid substitutions observed in Rhizocephala ETC genes could alternatively represent compensatory responses, relaxed selection, or a downregulation of bioenergetic activity, as seen in other anaerobically adapted eukaryotes (Müller et al. 2012). These alternative possibilities do not exclude adaptive evolution but rather emphasize that both adaptive and non-adaptive processes may have contributed to shaping mitochondrial genome evolution in Rhizocephala. The functional consequences of these putative selection signals should be validated through structural and biochemical assays. Nonetheless, our molecular and structural findings support the hypothesis that Rhizocephala species have undergone adaptive mitochondrial modifications in response to the metabolic constraints of parasitism. This study establishes a basis for future investigations into the functional consequences of these mutations and underscores the need to explore mito-nuclear coevolution within the oxidative phosphorylation pathway, particularly between mitochondrial and nuclear-encoded subunits, to fully understand their coordinated evolutionary consequences.

Conclusions

Our comparative study shows that parasitic Rhizocephala display accelerated mitochondrial genome evolution driven by both relaxed purifying selection and adaptive modifications. Non-adaptive processes likely predominate, yet positive selection in core ETC genes suggests that rhizocephalans have fine-tuned aspects of their respiratory machinery to thrive under host-mediated oxygen constraints. Extending these analyses to additional rhizocephalan taxa and integrating nuclear genome data will provide a richer picture of host–parasite coevolution at the molecular level. Further structural and functional studies of these ETC subunits are needed to clarify the mechanistic bases of rhizocephalan adaptation. Our findings highlight the complex mosaic of evolutionary forces—both genetic drift and selection—shaping the mtDNA of parasitic barnacles.

Materials and Methods

NGS Sequencing, Sequence Assembly, and Mitochondrial Genome Annotation

Samples for mitochondrial genome sequencing were isolated from their decapod hosts of each Rhizocephala species: *S. confragosa* (collected on 17 September 2020 from *Gaetice depressus*; GPS: 34.9°N, 128.1°E), *P. shiinoi* (collected on 17 September 2020 from *Upogebia major*; GPS: 34.9°N, 127.8°E), and *P. yatsui* (collected on 24 July 2017 from *Pachygrapsus crassipes*; GPS: 35.0°N, 139.8°E). Genomic DNA was extracted from the external tissues of a single adult individual (fixed in 95% ethanol) of each of the three rhizocephalan species using a DNeasy Blood & Tissue Kit (QIAGEN). The voucher specimens were deposited at the National Institute of Biological Resources, Korea, Coastal Branch of Natural History Museum and Institute, Chiba, Japan, and the Laboratory of Animal Phylogenomics at Ewha Womans University, Korea. Next-generation sequencing using a 150 bp paired-end library was performed by Illumina HiseqX Sequencer (Illumina, San Diego, CA). *De novo* assemblies were generated using both NOVOPlasty (Dierckxsens et al. 2017) and the CLC Genomics Workbench v6.5. The annotation of the assembled mitogenomes was performed in MITOS (http://mitos.bioinf.uni-leipzig.de/index.py; Bernt et al. 2013), with ORFs confirmed in Geneious Prime v.2022.0.1. The 13 PCGs were identified by sequence comparison with previously reported Cirripedia mtDNAs. Two rRNA genes (*rrnL, rrnS*) were confirmed via MITOS and comparisons with known cirriped sequences. tRNA genes were predicted using MITOS and their secondary structures were predicted using ARWEN (Laslett and Canbäck 2008) and edited by StructureEditor of RNA structure (Reuter and Mathews 2010).

Phylogenetic Analyses

We analyzed 45 complete mitochondrial genome sequences, including 42 Cirripedia species retrieved from GenBank and three newly sequenced rhizocephalans, using three crustacean species (*Squilloides leptosquilla*, *Gammarus pisinnus*, and *Portunus trituberculatus*) as outgroups (Table 3). Nucleotide composition bias and AT-skew (Perna and Kocher 1995) were calculated using MEGA12 (Kumar et al. 2024). Codon usage patterns of 13 PCGs of Rhizocephala and Thoracica were analyzed with the web-based program Sequence Manipulation Suite: Version 2 (http://www.geneinfinity.org/sms/sms_codonusage.html).

Nucleotide sequences of the 13 PCGs were individually aligned using Geneious Translation Align and subsequently concatenated for downstream analyses. Each PCG was treated as a separate data partition, and the best-fit substitution model

Downloaded from https://academic.oup.com/mbe/article/42/12/msaf303/8340872 by ewhalib - (INACTIVE) user on 18 May 2026

Table 3. Complete mitochondrial genomes used for phylogenetic and molecular sequence analyses in this study

Species	Infraclass	Order	Family	Size (bp)	Accession no.
Sacculina lata	Rhizocephala		Sacculinidae	14,579	MZ411548
Sacculina confragosa[a]				15,982	OQ129536
Parasacculina yatsui[a]			Polyascidae	16,005	OQ129535
Parasacculina shiinoi[a]				18,050	OQ129537
Polyascus gregarius				15,465	JN616263
Altiverruca navicula	Thoracica	Verrucomorpha	Verrucidae	15,976	MG252956
Capitulum mitella		Pollicipedomorpha	Pollicipedidae	14,915	MT439873
Pollicipes polymerus				15,634	AY456188
Lepas (*Anatifa*) *anatifera*		Scalpellomorpha	Lepadidae	15,708	ON060685
Lepas (*Anatifa*) *anserifera*				15,657	KP294311
Lepas (*Anatifa*) *australis*				15,502	KM017964
Vulcanolepas fijiensis			Neolepadidae	17,374	MN061491
Glyptelasma annandalei			Poecilasmatidae	16,107	MH891848
Arcoscalpellum epeeum			Scalpellidae	15,593	MH791047
Catomerus polymerus		Balanomorpha	Catophragmidae	15,447	MH791045
Chelonibia testudinaria			Chelonibiidae	14,906	KJ754819
Eochionelasmus coreana			Chionelasmatidae	17,035	MT491209
Eochionelasmus ohtai				15,585	MF939636
Nobia grandis			Pyrgomatidae	15,032	KF720334
Pyrgopsella youngi				15,129	MN615273
Savignium sp.				14,999	KJ754821
Epopella plicata			Tetraclitidae	15,296	KM008743
Tesseropora rosea				15,330	KY865099
Tetraclita japonica				15,192	MH119183
Tetraclita kuroshioensis				15,175	MW298526
Tetraclita rufotincta				15,002	KY865100
Tetraclita serrata				15,200	KJ434948
Tetraclita squamosa				15,191	MT232759
Tetraclitella divisa				14,973	KJ754822
Amphibalanus amphitrite			Balanidae	15,683	KF588709
Armatobalanus allium				15,063	KJ754817
Fistulobalanus albicostatus				15,665	MK617531
Semibalanus balanoides				15,119	MG010649
Semibalanus cariosus				15,118	MT528637
Striatobalanus amaryllis				15,064	KF493890
Balanus				15,955	KM660676
Balanus trigonus				15,560	MW646099
Acasta sulcata				15,326	KJ754818
Megabalanus ajax				15,510	KF501046
Megabalanus tintinnabulum				15,107	MN481499
Megabalanus volcano				15,107	AB167539
Notochthamalus scabrosus			Chthamalidae	15,397	KF425565
Octomeris sp.				15,484	KJ754820
Chthamalus antennatus				15,165	KP294312
Chthamalus challengeri				15,358	KY865097
Chthamalus malayensis				15,230	MW076458
Squilloides leptosquilla[b]	Hoplocarida	Stomatopoda	Squillidae	16,376	KR095170
Gammarus pisinnus[b]	Eumalacostraca	Amphipoda	Gammaridae	15,907	MK354236
Portunus trituberculatus[b]		Decapoda	Portunidae	16,017	MW232435

[a]Newly determined mitogenome in this study, [b]outgroups.

for each partition was identified based on the Bayesian Information Criterion using jModelTest v2.1.7 (Posada 2008). Maximum likelihood analysis with 1,000 bootstrap replicates were performed in RAxML v8.2.9 (Stamatakis 2014) on the CIPRES web portal (Miller et al. 2010).

Bayesian inference was conducted in MrBayes v3.2.6 (Huelsenbeck and Ronquist 2001) using Markov chain Monte Carlo with two independent runs of six chains, sampling every 100 generations for 1×10^6 generations. Stationarity and convergence of the MCMC chains were assessed using Tracer v1.7.1 (Rambaut et al. 2018), where all key parameters showed effective sample sizes > 200. Traces of likelihood and posterior probabilities were also visually inspected to confirm convergence. Bayesian posterior probability values were estimated after discarding the initial 2,000 trees as burn-in, once the parameter estimates had reached stationarity. To mitigate potential long-branch attraction, we applied the site-heterogeneous CAT model (Lartillot and Philippe 2004), excluded third codon positions, and removed long-branched Rhizocephala lineages to assess topological consistency. To evaluate the saturation of nucleotide sequences in the concatenated dataset, we generated saturation plots of transitions and transversions at each codon position (1st, 2nd, and 3rd) against genetic divergence based on TrN model distances in R (Everson 2015) (Fig. S7).

Two-cluster Test of Molecular Clock

To test whether Rhizocephala species evolve at different rates than Thoracica species in the 13 mitochondrial PCGs, we

Downloaded from https://academic.oup.com/mbe/article/42/12/msaf303/8340872 by ewhalib - (INACTIVE) user on 18 May 2026

performed a two-cluster test of the molecular clock using LINTRE (Takezaki et al. 1995). Due to clear evidence of substantial substitution saturation at the 3rd codon positions (Fig. S7), we excluded these positions from the DNA sequence alignment prior to downstream analyses in order to minimize the impact of potential homoplasy and phylogenetic noise. A neighbor-joining tree was reconstructed based on Kimura's two-parameter distance with variable base composition and gamma-distributed rate heterogeneity ("Kimura's two-parameter gamma" in LINTRE), using three crustacean species (*S. leptosquilla*, *G. pisinnus*, and *P. trituberculatus*) as outgroups. Based on the resulting neighbor-joining tree and substitution model, LINTRE tested whether the mean pairwise distances from the split node differed significantly between Rhizocephala and Thoracica lineages. To test whether the elevated substitution rates observed in mitochondrial genes also extend to the nuclear genome, we performed a two-cluster molecular clock test using nuclear 18S rDNA sequences, which represent both the most widely available and one of the most slowly evolving nuclear markers across Rhizocephala and Thoracica. For this analysis, we reconstructed an ML tree using IQ-TREE 2 (Minh et al. 2020), based on conserved regions extracted with Gblocks (Castresana 2000) from a multiple sequence alignment of the V5–V7 region of 18S rDNA sequences from 33 Rhizocephala and 32 Thoracica species using MEGA12 (Kumar et al. 2024) (Fig. S8). Because the 18S dataset lacked sufficient phylogenetic signal to recover monophyly of both target clades, we applied topological constraints enforcing monophyly of Rhizocephala and Thoracica based on established phylogenies. The resulting constrained ML tree was then used in LINTRE to perform a two-cluster clock test using the same analytical settings as in the mitochondrial analysis. This allowed direct comparison of substitution rates between the groups in both mitochondrial and nuclear genomes. Statistical significance of substitution rate differences between the two groups (Rhizocephala and Thoracica) was assessed using LINTRE's Z-test.

Selection Pressure Shift Analysis

To examine the shift in selection pressure among Rhizocephala species, we first used CodeML in PAML (Takezaki et al. 1995; Yang 2007) to estimate the nonsynonymous to synonymous substitution rates (d_N/d_S, ω) across the Cirripedia phylogeny under a free-ratio model (by setting model = 1, NSsite = 0, and fix_omega = 0 in the control file). To detect molecular signatures of relaxed or intensified purifying selection on each of 13 PCGs in the Rhizocephala species, we used RELAX (Wertheim et al. 2015) in HyPhy (Kosakovsky Pond et al. 2020), respectively. In this analysis, we specified the Rhizocephala clade as the "test" branches and the Thoracica clade as the "reference" branches to compare the relative strength of purifying selection between the two groups. A detailed description of the statistical framework is available on the HyPhy website (https://stevenweaver.github.io/hyphy-site/methods/selection-methods/). In brief, a statistically significant result with $K > 1$ indicates intensification, while $K < 1$ indicates relaxation of purifying selection along the test branches (Rhizocephala). To detect positive selection signals, we used BUSTED (Murrell et al. 2015) in HyPhy, which provides a gene-wide test for positive selection whether a gene has experienced positive selection at least one site on at least one branch. We designated the Rhizocephala clade as the foreground group and all remaining branches as the background group in this analysis.

Structural Modeling of Positively Selected Genes

The predicted structures of the three positively selected genes (Cyt *b*, Cox1, and Cox3) identified in Rhizocephala species were generated using AlphaFold2 (Jumper et al. 2021). Structural models were selected based on Predicted Local Distance Difference Test scores, retaining only those in the "very high" category (Predicted Local Distance Difference Test ≥ 90). Among these, the model with the lowest Predicted Alignment Error value was selected for downstream analysis. Structural analyses were conducted using PyMOL (Version 2.4.0, Schrödinger, LLC).

Supplementary Material

Supplementary material is available at *Molecular Biology and Evolution* online.

Acknowledgments

We thank Jongwoo Jung (Ewha Womans University) and Ryuta Yoshida (Ochanomizu University), who helped collect Rhizocephala samples for this study.

Author Contributions

J.J. and J.K.P. designed the study. J.J., J.K.P., S.S., M.Y.K., B.K.K.C., H.K., U.W.H., and S.S.C. analyzed and interpreted the data, and J.J., S.S., M.Y.K., U.W.H., and J.K.P. drafted the manuscript.

Funding

This research was supported by the National Research Foundation of Korea (NRF) grant funded by the Ministry of Science and ICT (MSIT) (No. 2020R1A2C2005393 to J.K.P.; No. RS-2022-NR070574 to S.S.C.; No. RS-2025-00561309 to U.W.H.).

Conflict of Interest

The authors declare that the research was conducted in the absence of any commercial or financial relationships that could be construed as a potential conflict of interest.

Data Availability

The original contributions presented in the study are included in the article/Supplementary Material. The raw NGS sequence data used for mitochondrial genome assembly have been deposited in the European Nucleotide Archive (ENA) under the accession number PRJEB102497. All relevant input data files and control files used in the analyses with RAxML, MrBayes, PAML, HyPhy, and LINTRE have been deposited in the Dryad Digital Repository (https://doi.org/10.5061/dryad.tx95x6b9w) to ensure reproducibility and public accessibility. Further inquiries can be directed to the corresponding author.

References

An J *et al.* Disrupted architecture and fast evolution of the mitochondrial genome of *Argeia pugettensis* (Isopoda): implications for speciation and fitness. *BMC Genomics*. 2020:21:1–14. https://doi.org/10.1186/s12864-020-07021-y.

Downloaded from https://academic.oup.com/mbe/article/42/12/msaf303/8340872 by ewhalib - (INACTIVE) user on 18 May 2026

Bernt M *et al*. MITOS: improved de novo metazoan mitochondrial genome annotation. *Mol Phylogenet Evol*. 2013:69:313–319. https://doi.org/10.1016/j.ympev.2012.08.023.

Bondareva OV, Potapova NA, Konovalov KA, Petrova TV, Abramson NI. Searching for signatures of positive selection in cytochrome b gene associated with subterranean lifestyle in fast-evolving arvicolines (Arvicolinae, Cricetidae, Rodentia). *BMC Ecol Evol*. 2021:21:92. https://doi.org/10.1186/s12862-021-01819-4.

Boore JL. Animal mitochondrial genomes. *Nucleic Acids Res*. 1999:27:1767–1780. https://doi.org/10.1093/nar/27.8.1767.

Bresciani J, Høeg JT. Comparative ultrastructure of the root system in rhizocephalan barnacles (Crustacea: Cirripedia: Rhizocephala). *J Morphol*. 2001:249:9–42. https://doi.org/10.1002/jmor.1039.

Bromham L. Why do species vary in their rate of molecular evolution? *Biol Lett*. 2009:5:401–404. https://doi.org/10.1098/rsbl.2009.0136.

Bromham L, Cowman PF, Lanfear R. Parasitic plants have increased rates of molecular evolution across all three genomes. *BMC Evol Biol*. 2013:13:126. https://doi.org/10.1186/1471-2148-13-126.

Castresana J. Selection of conserved blocks from multiple alignments for their use in phylogenetic analysis. *Mol Biol Evol*. 2000:17:540–552. https://doi.org/10.1093/oxfordjournals.molbev.a026334.

Chan BKK. Studies on *Tetraclita squamosa* and *Tetraclita japonica* (Cirripedia: Thoracica) II: larval morphology and development. *J Crustacean Biol*. 2003:23:522–547. https://doi.org/10.1651/C-2350.

Chan BKK *et al*. The evolutionary diversity of barnacles, with an updated classification of fossil and living forms. *Zool J Linn Soc*. 2021:193:789–846. https://doi.org/10.1093/zoolinnean/zlaa160.

Chan BKK, Poon DYM, Walker G. Distribution, adult morphology, and larval development of *Sacculina sinensis* (Cirripedia: Rhizocephala: Kentrogonida) in Hong Kong coastal waters. *J Crustacean Biol*. 2005:25:1–10. https://doi.org/10.1651/C-2495.

Chandel NS, Budinger GRS, Choe SH, Schumacker PT. Cellular respiration during hypoxia: role of cytochrome oxidase as the oxygen sensor in hepatocytes. *J Biol Chem*. 1997:272:111–112. https://doi.org/10.1074/jbc.272.30.18808.

da Fonseca RR, Johnson WE, O'Brien SJ, Ramos MJ, Antunes A. The adaptive evolution of the mammalian mitochondrial genome. *BMC Genomics*. 2008:9:119. https://doi.org/10.1186/1471-2164-9-119.

Darrouzet E, Valkova-Valchanova M, Moser CC, Dutton PL, Daldal F. Uncovering the [2Fe2S] domain movement in cytochrome bc1 and its implications for energy conversion. *Proc Natl Acad Sci U S A*. 2000:97:4567–4572. https://doi.org/10.1073/pnas.97.9.456.

Dierckxsens N, Mardulyn P, Smits G. NOVOPlasty: de novo assembly of organelle genomes from whole genome data. *Nucleic Acids Res*. 2017:45:e18. https://doi.org/10.1093/nar/gkw955.

Dowton M, Austin AD. Increased genetic diversity in mitochondrial genes is correlated with the evolution of parasitism in the Hymenoptera. *J Mol Evol*. 1995:41:958–965. https://doi.org/10.1007/BF00173176.

Ebert D. Experimental evolution of parasites. *Science*. 1998:282:1432–1436. https://doi.org/10.1126/science.282.5393.1432.

Everson K. Simple DNA saturation plots in R. 2015. Available from: https://www.kmeverson.org/blog/simple-dna-saturation-plots-in-r (accessed 25 June 2022).

Gillooly JF, Allen AP, West GB, Brown JH. The rate of DNA evolution: effects of body size and temperature on the molecular clock. *Proc Natl Acad Sci U S A*. 2005:102:140–145. https://doi.org/10.1073/pnas.0407735101.

Glenner H, Hebsgaard MB. Phylogeny and evolution of life history strategies of the parasitic barnacles (Crustacea, Cirripedia, Rhizocephala). *Mol Phylogenet Evol*. 2006:41:528–538. https://doi.org/10.1016/j.ympev.2006.06.004.

Golubinskaya DD, Korn OM, Sharina SN, Selin NI. Sympatric two-species infestation by rhizocephalan barnacle parasites in the spider crab *Pugettia aff. ferox* Ohtsuchi & Kawamura, 2019 from Peter the Great Bay (northwestern Sea of Japan). *Zool Stud*. 2021:60:54. https://doi.org/10.6620/ZS.2021.60-54.

Guzy RD, Schumacker PT. Oxygen sensing by mitochondria at complex III: the paradox of increased reactive oxygen species during hypoxia. *Exp Physiol*. 2006:91:807–819. https://doi.org/10.1113/expphysiol.2006.033506.

Hand SC, Hardewig I. Downregulation of cellular metabolism during environmental stress. *Annu Rev Physiol*. 1996:58:539–563. https://doi.org/10.1146/annurev.ph.58.030196.002543.

Hassanin A. Phylogeny of Arthropoda inferred from mitochondrial sequences: strategies for limiting the misleading effects of multiple changes in pattern and rates of substitution. *Mol Phylogenet Evol*. 2006:38:100–116. https://doi.org/10.1016/j.ympev.2005.09.012.

Hochachka PW, Buck LT, Doll CJ, Land SC. Unifying theory of hypoxia tolerance: molecular metabolic defense and rescue mechanisms for surviving oxygen lack. *Proc Natl Acad Sci U S A*. 1996:93:9493–9498. https://doi.org/10.1073/pnas.93.18.9493.

Høeg JT. Rhizocephala. In: Harrison FW, Humes AG, editors. *Microscopic anatomy of invertebrates, vol. 9, Crustacea*. Wiley; 1992. p. 313–345.

Høeg JT, Noever C, Rees DA, Crandall KA, Glenner H. A new molecular phylogeny-based taxonomy of parasitic barnacles (Crustacea: Cirripedia: Rhizocephala). *Zool J Linn Soc*. 2020:190:632–653. https://doi.org/10.1093/zoolinnean/zlz140.

Høeg JT, Pérez-Losada M, Glenner H, Kolbasov GA, Crandall KA. Evolution of morphology, ontogeny and life cycles within the Crustacea Thecostraca. *Arthropod Syst Phylog*. 2009:67:199–217. https://doi.org/10.3897/asp.67.e31697.

Huelsenbeck JP, Ronquist F. MRBAYES: Bayesian inference of phylogenetic trees. *Bioinformatics*. 2001:17:754–755. https://doi.org/10.1093/bioinformatics/17.8.754.

Jennings JB, Calow P. The relationship between high fecundity and the evolution of entoparasitism. *Oecologia*. 1975:21:109–115. https://doi.org/10.1007/BF00345553.

Jumper J *et al*. Highly accurate protein structure prediction with AlphaFold. *Nature*. 2021:596:583–589. https://doi.org/10.1038/s41586-021-03819-2.

Ki JS, Dahms HU, Hwang JS, Lee JS. The complete mitogenome of the hydrothermal vent crab *Xenograpsus testudinatus* (Decapoda, Brachyura) and comparison with brachyuran crabs. *Comp Biochem Physiol D: Genomics Proteomics*. 2009:4:290–299. https://doi.org/10.1016/j.cbd.2009.07.002.

Kosakovsky Pond SL *et al*. Hyphy 2.5-A customizable platform for evolutionary hypothesis testing using phylogenies. *Mol Biol Evol*. 2020:37:295–299. https://doi.org/10.1093/molbev/msz197.

Kumar S *et al*. MEGA 12: molecular evolutionary genetic analysis version 12 for adaptive and green computing. *Mol Biol Evol*. 2024:41:1–9. https://doi.org/10.1093/molbev/msae263.

Lartillot N, Philippe H. A Bayesian mixture model for across-site heterogeneities in the amino-acid replacement process. *Mol Biol Evol*. 2004:21:1095–1109. https://doi.org/10.1093/molbev/msh112.

Laslett D, Canbäck B. ARWEN: a program to detect tRNA genes in metazoan mitochondrial nucleotide sequences. *Bioinformatics*. 2008:24:172–175. https://doi.org/10.1093/bioinformatics/btm573.

Lin HC, Kobasov GA, Chan BKK. Phylogenetic relationships of Darwin's "Mr. Arthrobalanus": the burrowing barnacles (Cirripedia: Acrothoracica). *Mol Phylogenet Evol*. 2016:100:292–302. https://doi.org/10.1016/j.ympev.2016.03.016.

Luo Y *et al*. Mitochondrial genome analysis of *Ochotona curzoniae* and implication of cytochrome c oxidase in hypoxic adaptation. *Mitochondrion*. 2008:8:352–357. https://doi.org/10.1016/j.mito.2008.07.005.

Luong LT, Mathot KJ. Facultative parasites as evolutionary stepping-stones towards parasitic lifestyles. *Biol Lett*. 2019:15:20190058. https://doi.org/10.1098/rsbl.2019.0058.

Martínez Sosa F, Pilot M. Molecular mechanisms underlying vertebrate adaptive evolution: a systematic review. *Genes (Basel)*. 2023:14:416. https://doi.org/10.3390/genes14020416.

Miller MA, Pfeiffer W, Schwartz T. Creating the CIPRES Science Gateway for inference of large phylogenetic trees. In: *2010 Gateway computing environments workshop (GCE)*. IEEE; 2010. p. 1–8.

Downloaded from https://academic.oup.com/mbe/article/42/12/msaf303/8340872 by ewhalib - (INACTIVE) user on 18 May 2026

Minh BQ *et al*. IQ-TREE 2: new models and efficient methods for phylogenetic inference in the genomic era. *Mol Biol Evol*. 2020:37:1530–1534. https://doi.org/10.1093/molbev/msaa015.

Miroliubov A *et al*. Specialized structures on the border between rhizocephalan parasites and their host's nervous system reveal potential sites for host-parasite interactions. *Sci Rep*. 2020:10:1128. https://doi.org/10.1038/s41598-020-58175-4.

Miroliubov AA *et al*. Muscular system in the interna of *Polyascus polygenea* and *Sacculina pilosella* (Cirripedia: Rhizocephala: Sacculinidae). *Invert Zool*. 2019:16:48–56. https://doi.org/10.15298/invertzool.16.1.06.

Miroliubov AA *et al*. The interna of the rhizocephalan *Peltogaster reticulata*: comparative morphology and ultrastructure. *Arthropod Struct Dev*. 2022:70:101190. https://doi.org/10.1016/j.asd.2022.101190.

Müller M *et al*. Biochemistry and evolution of anaerobic energy metabolism in eukaryotes. *Microbiol Mol Biol Rev*. 2012:76:444–495. https://doi.org/10.1128/MMBR.05024-11.

Murrell B *et al*. Gene-wide identification of episodic selection. *Mol Biol Evol*. 2015:32:1365–1371. https://doi.org/10.1093/molbev/msv035.

O'Brien J, Van Wyk P. Effects of crustacean parasitic castrators (epicaridean isopods and rhizocephalan barnacles) on growth of crustacean hosts. In: *Crustacean issues 3*. Routledge; 1985. p. 191–218.

Ohta T. Slightly deleterious mutant substitutions in evolution. *Nature*. 1973:246:96–98. https://doi.org/10.1038/246096a0.

Øksnebjerg B. The Rhizocephala (Crustacea: Cirripedia) of the Mediterranean and Black Seas: taxonomy, biogeography, and ecology. *Isr J Zool*. 2000:46:1–102. https://doi.org/10.1560/RCLC-NM2U-HV5L-6Q52.

Page RD, Lee PL, Becher SA, Griffiths R, Clayton DH. A different tempo of mitochondrial DNA evolution in birds and their parasitic lice. *Mol Phylogenet Evol*. 1998:9:276–293. https://doi.org/10.1006/mpev.1997.0458.

Park JK *et al*. A common origin of complex life cycles in parasitic flatworms: evidence from the complete mitochondrial genome of *Microcotyle sebastis* (Monogenea: Platyhelminthes). *BMC Evol Biol*. 2007:7:11. https://doi.org/10.1186/1471-2148-7-11.

Pérez-Losada M, Høeg JT, Crandall KA. Remarkable convergent evolution in specialized parasitic Thecostraca (Crustacea). *BMC Biol*. 2009:7:1–12. https://doi.org/10.1186/1741-7007-7-15.

Perna NT, Kocher TD. Patterns of nucleotide composition at fourfold degenerate sites of animal mitochondrial genomes. *J Mol Evol*. 1995:41:353–358. https://doi.org/10.1007/BF00186547.

Podsiadlowski L, Bartolomaeus T. Organization of the mitochondrial genome of mantis shrimp *Pseudosquilla ciliata* (Crustacea: Stomatopoda). *Mar Biotechnol*. 2005:7:618–624. https://doi.org/10.1007/s10126-005-0017-8.

Posada D. jModelTest: phylogenetic model averaging. *Mol Biol Evol*. 2008:25:1253–1256. https://doi.org/10.1093/molbev/msn083.

Poulin R. *Evolutionary ecology of parasites*. 2nd ed. Princeton University Press; 2011. p. 1–360.

Rambaut A, Drummond AJ, Xie D, Baele G, Suchard MA. Posterior summarization in Bayesian phylogenetics using tracer 1.7. *Syst Biol*. 2018:67:901–904. https://doi.org/10.1093/sysbio/syy032.

Reuter JS, Mathews DH. RNA structure: software for RNA secondary structure prediction and analysis. *BMC Bioinf*. 2010:11:129. https://doi.org/10.1186/1471-2105-11-129.

Sazanov LA. A giant molecular proton pump: structure and mechanism of respiratory complex I. *Nat Rev Mol Cell Biol*. 2015:16:375–388. https://doi.org/10.1038/nrm3997.

Schram FR. *Crustacea, xiv*. Oxford University Press; 1986. p. 1–606.

Sharma V, Jambrina PG, Kaukonen M, Rosta E, Rich PR. Insights into functions of the H channel of cytochrome c oxidase from atomistic molecular dynamics simulations. *Proc Natl Acad Sci U S A*. 2017:114:E10339–E10348. 10.1073/pnas.1708628114.

Shokri Bousjein N, Gardner MG, Schwarz MP. Small effective population sizes of bee social parasites compared to their hosts raise important questions for evolutionary arms race. *J Zool*. 2016:299:17–26. 10.1111/jzo.12325.

Spears T, Abele LG, Applegate MA. Phylogenetic study of cirripedes and selected relatives (Thecostraca) based on 18S rDNA sequence analysis. *J Crustacean Biol*. 1994:14:641–656. https://doi.org/10.1163/193724094X00614.

Stamatakis A. RAxML version 8: a tool for phylogenetic analysis and post-analysis of large phylogenies. *Bioinformatics*. 2014:30:1312–1313. https://doi.org/10.1093/bioinformatics/btu033.

Strobel HM, Hays SJ, Moody KN, Blum MJ, Heins DC. Estimating effective population size for a cestode parasite infecting three-spined sticklebacks. *Parasitology*. 2019:146:883–896. https://doi.org/10.1017/S0031182018002226.

Takezaki N, Rzhetsky A, Nei M. Phylogenetic test of the molecular clock and linearized trees. *Mol Biol Evol*. 1995:12:823–833. https://doi.org/10.1093/oxfordjournals.molbev.a040259.

Timón-Gómez A, Bartley-Dier EL, Fontanesi F, Barrientos A. HIGD-driven regulation of cytochrome c oxidase biogenesis and function. *Cells*. 2020:9:2620. https://doi.org/10.3390/cells9122620.

Trouvé S, Sasal P, Jourdane J, Renaud F, Morand S. The evolution of life-history traits in parasitic and free-living platyhelminthes: a new perspective. *Oecologia*. 1998:115:370–378. https://doi.org/10.1007/s004420050530.

Weinstein SB, Kuris AM. Independent origins of parasitism in Animalia. *Biol Lett*. 2016:12:20160324. https://doi.org/10.1098/rsbl.2016.0324.

Wertheim JO, Murrell B, Smith MD, Kosakovsky Pond SL, Scheffler K. RELAX: detecting relaxed selection in a phylogenetic framework. *Mol Biol Evol*. 2015:32:820–832. https://doi.org/10.1093/molbev/msu400.

Wolstenholme DR. Animal mitochondrial DNA: structure and evolution. *Int Rev Cytol*. 1992:141:173–216. https://doi.org/10.1016/S0074-7696(08)62066-5.

Xiao JH, Jia JG, Murphy RW, Huang DW. Rapid evolution of the mitochondrial genome in chalcidoid wasps (Hymenoptera: Chalcidoidea) driven by parasitic lifestyles. *PLoS One*. 2011:6:e26645. https://doi.org/10.1371/journal.pone.0026645.

Xu SQ *et al*. A mitochondrial genome sequence of the Tibetan antelope *Pantholops hodgsonii*. *Genomics Proteomics Bioinformatics*. 2005:3:5–17. https://doi.org/10.1016/S1672-0229(05)03003-2.

Yang JS, Yang WJ. The complete mitochondrial genome sequence of the hydrothermal vent galatheid crab *Shinkaia crosnieri* (Crustacea: Decapoda: Anomura): a novel arrangement and incomplete tRNA suite. *BMC Genomics*. 2008:9:257. https://doi.org/10.1186/1471-2164-9-257.

Yang M, Gong L, Sui J, Li X. The complete mitochondrial genome of *Calyptogena marissinica* (Heterodonta: Veneroida: Vesicomyidae): insight into the deep-sea adaptive evolution of vesicomyids. *PLoS One*. 2019:14:e0217952. https://doi.org/10.1371/journal.pone.0217952.

Yang Z. PAML 4: phylogenetic analysis by maximum likelihood. *Mol Biol Evol*. 2007:24:1586–1591. https://doi.org/10.1093/molbev/msm088.

Zdorevskyi O, Djurabekova A, Lasham J, Sharma V. Horizontal proton transfer across the antiporter-like subunits in mitochondrial respiratory complex I. *Chem Sci*. 2023:14:6309–6318. https://doi.org/10.1039/D3SC01427D.

Zhang B *et al*. Comparative analysis of mitochondrial genome of a deep-sea crab *Chaceon granulates* reveals positive selection and novel genetic features. *J Oceanol Limnol*. 2020:38:427–437. https://doi.org/10.1007/s00343-019-8364-x.

Zhang K, Sun J, Xu T, Qiu JW, Qian PY. Phylogenetic relationships and adaptation in deep-sea mussels: insights from mitochondrial genomes. *Int J Mol Sci*. 2021:22:1900. https://doi.org/10.3390/ijms22041900.

Downloaded from https://academic.oup.com/mbe/article/42/12/msaf303/8340872 by ewhalib - (INACTIVE) user on 18 May 2026